An Enhanced Faraday Cup for Rapid Determination of Power Density Distribution in Electron Beams

An improved Faraday cup promises to provide rapid and accurate beam profiles, eliminating sources of error that are detrimental to a production environment

BY J. W. ELMER AND A. T. TERUYA

ABSTRACT. Enhancements have been made to a modified Faraday cup (MFC) diagnostic device for measuring the power density distribution of high-power electron beams used for welding. The modifications consist of additions to the hardware components of a previously developed MFC for more complete capture of the electrons, better electrical grounding, and the addition of a new method for orienting the measured beam profile with respect to the coordinates of the welding chamber. These modifications improve the quality of the acquired data and enable a more accurate computed tomographic (CT) reconstruction of power density distribution of the electron beam than has been possible in the past. Comparisons were made between previous and enhanced versions of the MFC. Results demonstrated improved electron capture and improved signal-to-noise ratio with the new design, allowing the acquired beam profile to be CT reconstructed without noise filtering. In addition, Gaussian distributed beams were used to simulate beam profiles acquired by the MFC diagnostic as a function of the finite width of the slits used to measure beam properties. From these simulations, the amount of error in the beam profile introduced by the slits was determined and a method for compensating for this error proposed.

Introduction

The diagnostics necessary to repeatedly produce a focused beam of known power density are not currently available on commercial electron beam welding machines. Rather, the beam focus is operator dependent and influenced by the desired welding parameters and machine characteristics (Refs. 1–9).

A diagnostic tool for rapidly measuring the power-density distribution of electron beams is currently under development. This technique uses a modified Faraday cup technique and employs a tungsten disk with regularly spaced radial slits (Refs. 8–9) to sample the electron beam. This diagnostic technique captures multiple beam profiles in a fraction of a second as the beam is oscillated in a circular pattern over the tungsten disk. These individual beam profiles are then reconstructed using a computed tomographic method to render an image of the beam shape, size, and power density distribution (Ref. 10). All this data is gathered and processed in less than a minute, making this technique very attractive for eventual use in production environments. The speed and ease of use of this diagnostic will eventually provide welding operators with the ability to acquire a permanent quality control record of the beam, to repeat welds on the same machine over a period of time, and to transfer welding parameters between machines and facilities.

This diagnostic technique needs to be robust, reliable, and must provide dependable data with minimal decision-making on the part of the welding operator for acceptance in a production environment. In the previous MFC design, the beam current passing through the slit was sampled using an otherwise conventional Faraday cup (Ref. 8).

Although this technique worked well, the overall design required improvement in several areas. First, since a portion of the beam's current passing into the Faraday cup could be transported out of the cup and back to the tungsten slit as backscattered electrons, this portion of the beam's current would not be properly accounted for by the diagnostic. Second, with repeated use, the electrical contact between the tungsten slit disk and the copper heat sink body could degrade, adding electronic noise to the measured beam profiles. Third, the beam orientation was determined using one slit that was twice as wide as the others, which created an unnecessary error in the wide-slit profile.

Although these sources of errors do not pose serious problems in a research and development environment, they would create unnecessary complications in a production environment. This paper describes enhancements made to the MFC to help minimize these potential sources of error and to make measurements more reliable.

KEY WORDS

Faraday Cup
Electron Beam Welding
Computed Tomography
Diagnostics
Power Density
Gaussian Distribution
Beam Focus

Experimental Procedures

Enhancements to the Modified Faraday Cup

Figure 1 shows a schematic of the MFC diagnostic's original design. This device consists of a copper Faraday cup within an electrically insulating ceramic cup, a tungsten disk containing 17 slits, and a cylindrical copper heat sink that

J. W. ELMER and A. T. TERUYA are with Lawrence Livermore National Laboratory, Livermore, Calif.

holds the tungsten disk above the Faraday cup (Ref. 8).

During operation, the electron beam deflection coils are used to sweep the beam in a circle of known diameter at a constant frequency over the tungsten slit disk. The majority of the beam's current is intercepted by the tungsten disk and conducted by the copper heat sink to ground. However, when the beam passes over a slit, a portion of the beam current passes through the slit and into the Faraday cup where it can be measured as a voltage drop across a known resistor.

A current vs. time profile is collected using a fast-sampling, analog-to-digital (A/D) converter as the beam passes over each slit. This beam profile information is stored on a personal computer, which later reconstructs the power-density distribution in the beam. The tungsten disk (38-mm diameter and 2.5 mm thick) containing the 17 radially positioned slits was manufactured by electro-discharge machining (EDM) using a 0.1-mm-diameter wire. A 3.0-mm-diameter hole is further machined through the center of the disk, which allows a sharp focused spot beam to pass entirely through the tungsten disk and into the Faraday cup to measure the full beam current.

Incomplete electron capture and signal degradation after repeated use of the MFC were observed while using the original MFC diagnostic, and the following changes were made to the diagnostic to minimize these errors.

Electron capture was improved through several modifications that were made to the MFC hardware, as illustrated in Fig. 2. First, an additional slit disk, made of copper, was added to the top of the internal Faraday cup. This copper slit disk captured the majority of backscattered electrons and prevented them from leaving the Faraday cup. Second, a beam trap was added inside of the MFC to provide even more containment of the electron beam when the full beam current was measured through the center hole of the MFC. Third, a graphite ring was added below the copper slit disk, and a graphite disk added at the bottom of the beam trap to minimize the amount of backscattered electrons that passed through the slits.

To improve grounding of the tungsten slit disk, a 0.020-in.-diameter tantalum wire was vacuum brazed to the tungsten slit disk then attached to the copper heat sink body. That way, if the copper heat sink became oxidized with repeated use, there would still be a low-resistance electrical path from the tungsten slit disk to ground. In addition, a copper clamp was employed to maintain pressure on the tungsten slit disk for maintaining good electrical and thermal contact with the heat sink body.

The final enhancement was to change the method for determing beam orientation. Previously (Ref. 8), one of the 17 slits in the tungsten disk was made twice as wide as the others to provide one large profile in the captured waveform to indicate the beam's orientation. In the new design, two adjacent, wide-spaced slits produced one wide temporal gap in the 17-peak waveform for proper orientation of the beam. This allowed all slits to be machined with the same (small) width and reduced the error introduced by the previously used wide slit while still maintaining a method for determining the beam's orientation.

Data Acquisition and Computed Tomographic Imaging

Data acquisition was performed as before (Ref. 10) using an A/D converter and a personal computer running *LabView* software (Ref. 11). Data was acquired as a voltage drop across a 210-W resistor,

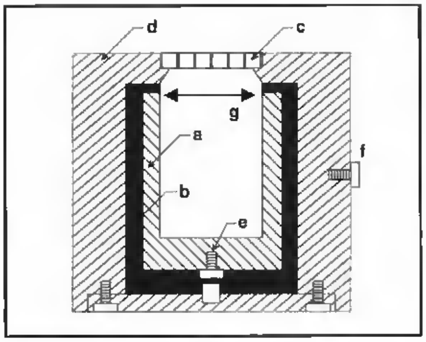

Fig. 1 — Cross-sectional illustration of the original MFC diagnostic. Copper Faraday cup (a) is surrounded by an insulating ceramic cup (b). The tungsten slit disk (c) is centered over the Faraday cup and supported by the outer copper heat sink (d). The signal from the Faraday cup is carried through a wire attached to lug (e) and the remainder of the beam's current is carried directly to ground through a wire attached to lug (f). The interior allows backscattered electrons to exit the Faraday cup through the opening (g) below the slit disk.

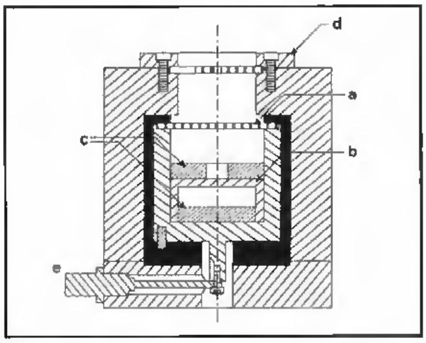

Fig. 2 — Cross-sectional illustration of the enhanced MFC diagnostic. Enhancements include the following: (a) an internal slit disk made of copper; (b) an internal beam trap; (c) graphite beam interceptors; (d) a clamp for the tungsten slit disk; and (e) an integral BNC connector. The ground wire from the tungsten slit disk to the heat sink body is not shown.

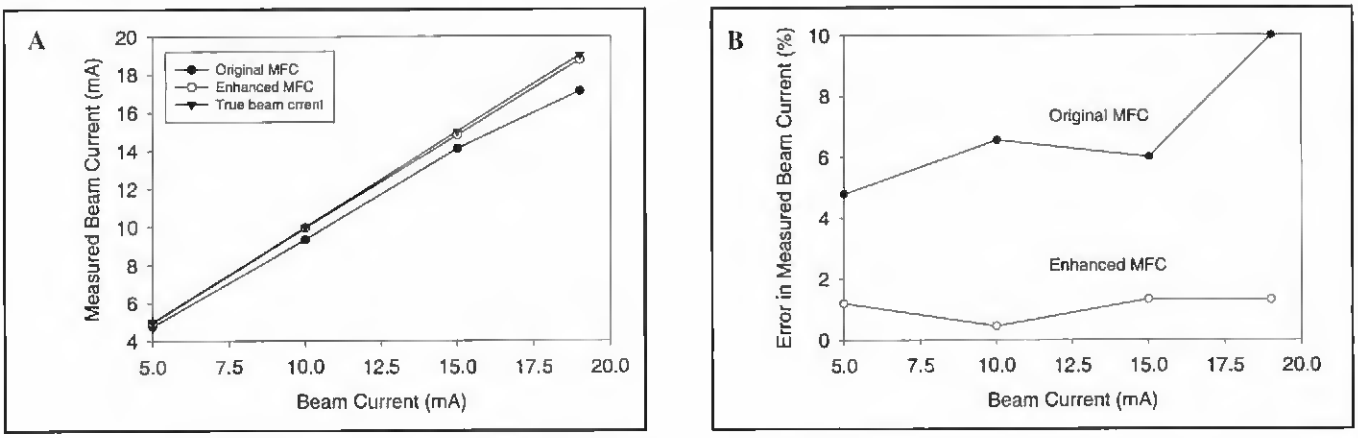

Fig. 3 — A — Comparison of the total beam current measured by the original and enhanced MFCs with the true beam current; B — the percentage error in the measured total beam current for the original and enhanced MFCs.

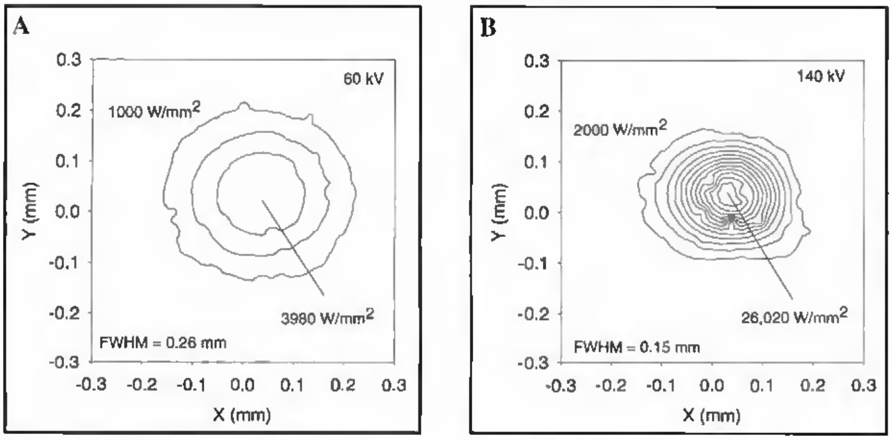

Fig. 4 — Tomographic reconstructions of a sharp-focused, 5-mA beam. A — 60 kV; B — 140-kV accelerating voltages. The 140-kV beam has a significantly smaller FWHM, resulting in a peak power density that is 6.5 times greater than that of the 60-kV beam. These reconstructions have not been corrected for slit width related errors.

which was then converted into a digital signal with the A/D converter sampling at 500 kHz. In this study, the electron beam was swept around a 25.4-mm-diameter circle at 30 Hz. The digital waveform containing the 17 consecutive beam profiles was created as the beam passed over the slits and was captured in 35 ms.

CT reconstruction of power distribution in the beam was performed using *LabView* running a custom-designed CT program on the same personal computer that acquired the data. The beam profile conditioning and tomographic reconstruction algorithm have been previously discussed (Refs. 8–10). This algorithm consists of separating individual beam profiles, normalizing areas under the peaks, filtering this data if necessary, creating a sinogram from the series of profiles, CT reconstructing the power density distribution, and calculating the beam's power density distribution. A 128 x 128 pixel reconstruction of this beam took approximately 10 s to perform and display on a Pentium-based laptop personal computer.

Some modifications were made to the CT algorithm to reconstruct data from the new tungsten slit disk having one wide-spaced set of slits rather than one wide slit as used in the past. In addition, the computer tomography algorithm was modified to account for reconstruction artifacts caused by the small number of beam profiles gathered by the 17-slit tungsten disk. This modification allowed more accurate reconstructions to be performed than before and resulted in higher calculated peak power densities than previously reported.

Results and Discussion

Electron beams were investigated using both original and enhanced MFCs. The total beam current and power-density distribution were measured for electron beams generated by a 150-kV/50-mA Hamilton Standard (HS) welding machine (Serial Number 175) fitted with a ribbon filament and an R-40 gun. Work distance was kept constant at 178 mm from the top of the chamber, and the vacuum level in the chamber was maintained at 1×10^{-5} torr. Power density distribution measurements were made on 5-mA beams at 140 kV, which is a convenient power level to use since special precautions are not required to prevent melting of the tungsten slit disk.

Enhanced Electron Capture

To demonstrate the improved electron capture of the enhanced MFC, sharp-focused beams were examined to measure the beam current using each MFC design. In this set of experiments, both 60-kV and 140-kV beams were examined for a range of beam currents from 5 to 19 mA. These experiments measured the total beam current as it passed through the center hole of both the original and enhanced MFCs. Results of these measurements are summarized in Table 1 and plotted in Fig. 3A, showing the beam current measured by the enhanced MFC is closer to the true machine value than that measured by the original MFC. These data are further compared in Fig. 3B, where the percentage error in the measured beam current values are plotted. Here, the percentage error is calculated from the difference between the measured value and the value set on the electron beam welding machine, and is the average of the measured values at 60 and 140 kV. This error represents the percent of the true beam current that is not accounted for by the MFC diagnostic. The error is largest for the original MFC,

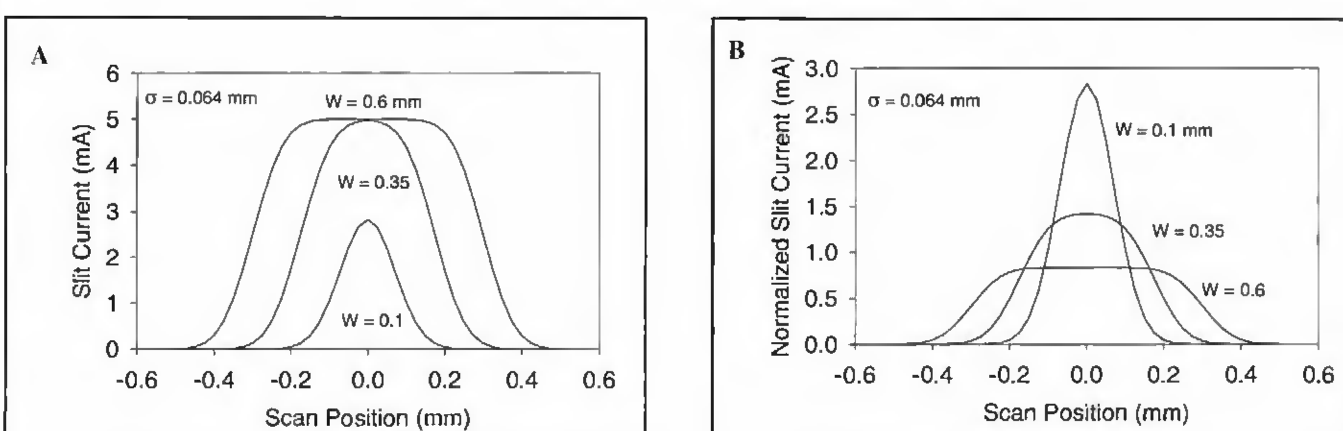

Fig. 5 — Simulated beam profiles for a Gaussian-distributed, 5-mA beam with a FWHM of 0.15 mm (σ = 0.064 mm) passing over slits of three different widths. A — Comparison of the total slit current as a function of beam position. B — Comparison of the normalized values where all profiles have the same area.

which varies between 5 and 10% of the total beam current, whereas the enhanced MFC is relatively consistent and shows less than a 1.5% error in the measured beam current.

Even with the enhancements made to the MFC, the beam current is being underestimated by about 1% on average. This underestimation of the beam current is related to the width of the slits in the copper slit disk and the geometry of the beam trap, which still allows some backscattered electrons to escape from the cup. Reducing the slit widths of the copper slit disk and the diameter of the hole in the beam trap will further improve electron capture with the enhanced MFC if more precise beam current measurements are required from the MFC diagnostic.

Table 1 — Comparison of Measured Beam Current between Original MFC and Enhanced MFC for Different Beams

True Beam Current (mA)	Accelerating Voltage 1 60kV Original MFC (mA)	Accelerating Voltage 1 60kV Enhanced MFC (mA)	Accelerating Voltage 2 140kV Original MFC (mA)	Accelerating Voltage 2 140kV Enhanced MFC (mA)
5	4.77	4.98	4.75	4.90
10	9.34	9.91	9.35	10.0
15	14.1	14.8	14.1	14.8
19	17.8	18.7	16.4	18.8

EB Welding Machine HS No. 175.

Table 2 — Comparison of Measured Electron Beam Properties

Beam Property	EB Welding Machine No. 175 60 kV	EB Welding Machine No. 175 140 kV	EB Welding Machine No. 605 80 kV	EB Welding Machine No. 605 140 kV
Peak (kW/mm^2)	3.98	26.0	2.87	7.92
FWHM (mm)	0.26	0.15	0.36	0.28
1/e^2 (mm)	0.42	0.26	0.61	0.45
σ (mm)	0.11	0.064	0.15	0.12

Note: Sharp-focused, 5-mA beams for two different welding machines and for different accelerating voltages.

The Effect of Slit Width on the Measured Power Density Distribution

The present version of the CT reconstruction algorithm assumes that the width of the slit is small compared to the diameter of the beam and can therefore be neglected. This assumption is reasonably valid for defocused beams where the ratio of slit width to beam diameter is small. However, for sharp-focused beams where the finite slit width represents a larger fraction of the beam's diameter, the diagnostic will overestimate the beam's diameter and thus underestimate the peak power density of the beam. The amount of error introduced by the finite width of the slit can be calculated for Gaussian distributed beams, which is useful for selecting the appropriate slit width for a given beam.

Since the amount of error in the measured power density distribution depends on both slit width and beam size, simulations were performed using sharp-focused beams to calculate the worst-case scenario (highest error introduced by a given slit) that we expect to measure with the CT diagnostic technique. Furthermore, since the beam size depends on accelerating voltage (Ref. 8) and electron optics, we measured the beam size for different accelerating voltages and on two different welding machines. These data are summarized in Table 2 for sharp-focused, 5-mA beams. Some of this data was previously obtained from Hamilton Standard EB welding machine No. 605 (Ref. 8), showing that the beam on this machine is full width at half maximum (FWHM) at 0.36 mm at 80 kV, and a smaller FWHM of 0.28 mm at 140 kV.

A similar comparison was made in the present investigation using Hamilton Standard welding machine No. 175. Figure 4 shows one result from this study, comparing the tomographic reconstructions of the 60- and 140-kV beams. Here, the sharp-focused beams were measured to have a FWHM of 0.26 and 0.15 mm for the 60- and 140-kV voltages, respectively. For both welding machines, the beam became smaller as the voltage was increased, showing that higher voltage beams focus to smaller spot sizes than lower voltage beams for a given electron beam welding machine. In addition, the comparison between the two welding machines shows that HS welding machine No. 175 focuses to a smaller spot size than HS welding machine 605 at a given beam voltage.

The smallest measured beam size in this study was a 5-mA, 140-kV beam on HS No. 175, which had a CT-reconstructed FWHM of only 0.15 mm. This beam was chosen for the calculations that follow for estimating the maximum error introduced by the finite slit width into the CT reconstructions for these machines. In these calculations, the beam profile measured by the diagnostic is simulated by passing a Gaussian distributed beam over a slit of a given width. The error introduced by the finite width of the slit can then be calculated from the difference between the simulated beam profile and the true beam profile. This simulation assumes the electron beam has a circular Gaussian distribution that most closely represents the sharp-focused beam condition represented by the following equation (Ref. 9):

$$J(x,y) = \frac{I}{2\pi\sigma^2} \exp\left[\left(\frac{-x^2}{2\sigma^2}\right) + \left(\frac{-y^2}{2\sigma^2}\right)\right] \quad (1)$$

where J(x,y) is the current density of the beam, σ is the standard deviation of the Gaussian distribution, I is the total beam current, and x and y are rectangular spatial coordinates. For a beam moving in the positive x-direction and perpendicular to the slit, the instantaneous current passing through the slit as a function of position, $I_S(x)$, can be calculated. This calculation is performed by integrating the current density distribution given by equation 1 along the y direction for a slit of width w as follows:

$$I_s(x) = \frac{I}{2\pi\sigma^2} \int_{x-\frac{w}{2}}^{x+\frac{w}{2}} \int_{-\infty}^{+\infty} \exp\left[\left(\frac{-x^2}{2\sigma^2}\right) + \left(\frac{-y^2}{2\sigma^2}\right)\right] dx\, dy \quad (2)$$

Equation 2 was integrated using *MathCad* (Ref. 12) for a series of simulated slit widths between 0.01 and 1 mm. This range of slit widths more than spans the range of slit widths used for electron beam tomography, which are typically on the order of 0.1 mm wide (Refs. 8, 9).

Figure 5A compares the results of three simulated beam profiles as the

RESEARCH/DEVELOPMENT/RESEARCH/DEVELOPMENT/RESEARCH/DEVELOPMENT/RESEARCH/DEVELOPMENT

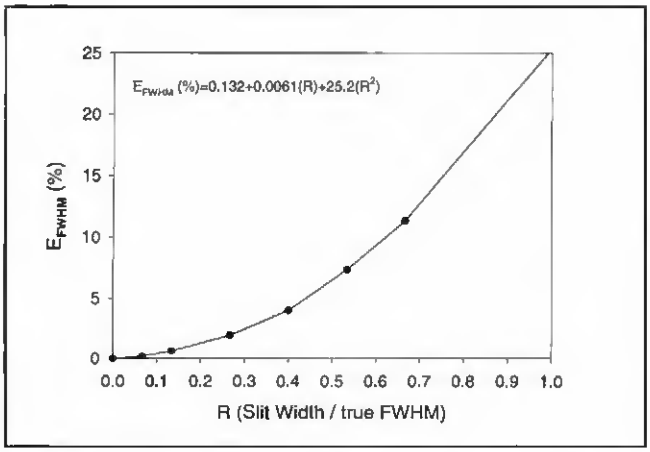

Fig. 6 — *Calculated error of the FWHM as a function of slit width up to the true FWHM of the beam.*

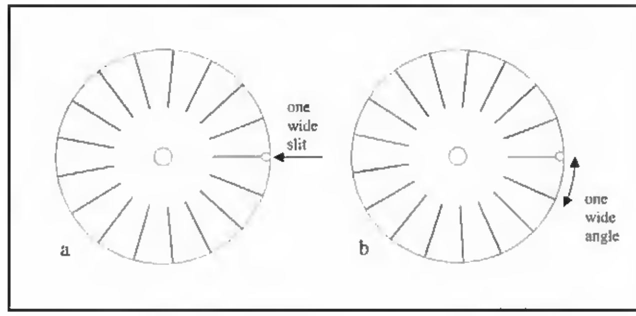

Fig. 7 — *A — Illustration of the original slit disk where one slit is machined to be twice as wide (0.2 mm) as the remaining 16 slits, but all slits are equally spaced at 21.18 deg. B — Illustration of the new design where all slits are machined with the same width (0.1 mm), but one set of slits has a wide spacing (24 deg) and the remaining slits are equally spaced at 21 deg. The small hole on the outside of the slit disk is used for alignment purposes, while the hole in the center is used to measure the full beam current.*

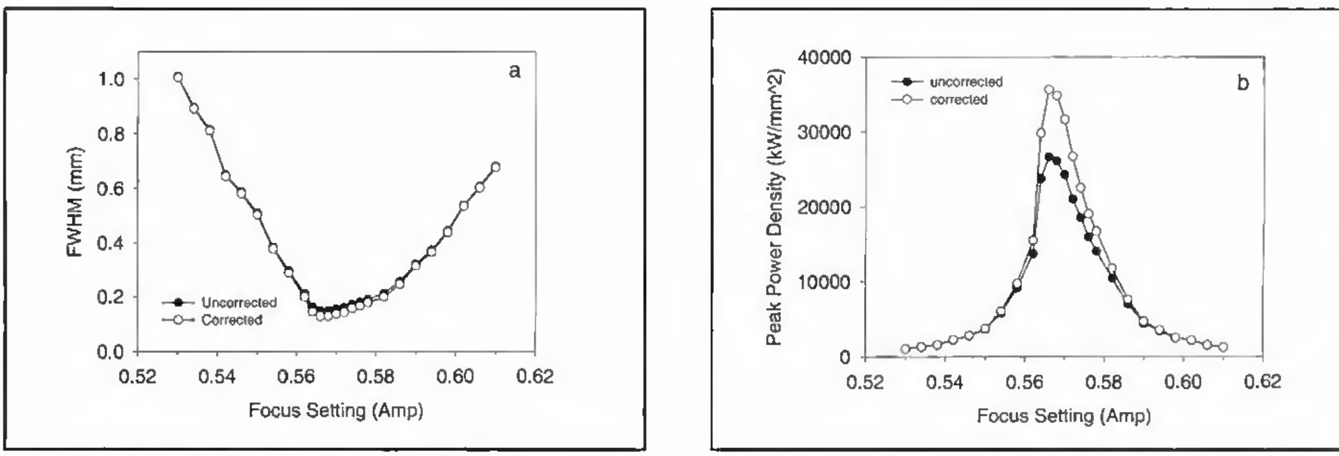

Fig. 8 — *Results of the defocus study for the140-kV, 5-mA beam. A — Plots of the FWHM for the tomographically reconstructed data (solid circles) and the slit width corrected data (open circles); B — plots of the same for peak power density measurements.*

beam passes over slits 0.6, 0.35, and 0.1 mm wide. The 0.15-mm FWHM beam is significantly smaller than the 0.6-mm-wide slit, therefore, the entire beam passes through this slit for a period of time, creating a flat-topped shape to the beam profile. This slit is clearly too wide to be used for tomography since it would average out any beam inhomogeneities that exist.

The slit current as measured by the 0.35-mm-wide slit is Gaussian shaped and nearly reaches the full beam current when the beam is centered over the slit. As will be shown later, the 0.35-mm slit would overestimate the measured FWHM of this beam by a significant amount, and is therefore considered to be too wide for CT reconstruction.

The slit current, as measured by the 0.1-mm-wide slit, is also Gaussian shaped, but allows a much lower percentage of the beam to pass through the slit. This is the preferred slit width for tomography, because it allows the beam's shape to be measured with higher precision. Although smaller slit widths would provide an even more precise measurement of the beam shape in theory, practical considerations created by the high aspect ratio of these slits (tungsten thickness/slit-width), the reduced slit current, and fabrication considerations make slits smaller than 0.1 mm difficult to work with.

The beam profiles shown in Fig. 5A contain significantly different areas because wider slits allow more electrons to pass through. So, these raw beam profiles need to be normalized to account for their different areas and for comparisons to be made. This type of normalization is also required in the CT reconstruction program due to inherent variations in slit widths (Refs. 8–10). Figure 5B shows what these normalized beam profiles look like after being divided by their respective areas so all contain the same unit area.

It is clear from the results shown in Fig. 5B that the FWHM of the normalized beam profiles increase as the width of the slit increases, and the widest slit would result in the lowest peak power density measurement for a given beam. Since the amount of error in the measured beam depends not only on the slit width but also on the beam size, it is important to understand how the percentage error in the measured FWHM of the beam varies as a function of both parameters.

In the calculations that follow, the error in the FWHM measurement was determined for Gaussian-shaped beams using a ratio, R, of the slit width to the true FWHM of the beam. Here, the true FWHM of the beam is smaller than the beam profile measured using the MFC, which will be discussed in more detail later.

Simulations of beam profiles were made for a 0.15-mm FWHM beam using different slit widths up to the FWHM of the beam, *i.e.*, for $0<R<1$. Figure 6 plots these results, showing a nonlinear increase in the error as R increases. The error in the measured FWHM of the beam can be quite large, exceeding 20% as the slit width approaches the FWHM of the beam, but drops off to values less than 5% for $R < 0.33$. These data were fit to a second order polynomial to determine a predictive relationship between R and the percentage error in the FWHM measurement, E_{FWHM}, as follows:

$$E_{FWHM}(\%) = 0.132 + 0.0061(R) + 25.2(R)^2 \quad (3)$$

where the variables E_{FWHM} (%) and R are defined as

$$E_{FWHM}(\%) = 100^{*}(\text{FWHM measured} - \text{FWHM true})/\text{FWHM true} \quad (4)$$

$$R = (\text{slit width})/(\text{FWHM true}) \quad (5)$$

Using these relationships, the percentage error introduced by tungsten slits of 0.1 and 0.2 mm were calculated for different beams. These slits represent the two different sizes used in the original tungsten slit disk design whereby 16 small slits (0.1 mm) and one large slit (0.2 mm) were used for beam orientation purposes. Four different beam sizes were investigated as well, representing two different accelerating voltages on HS Nos. 175 and 605 welding machines.

Table 3 summarizes the results of these calculations. In this table, the measured FWHM data are the FWHM values as experimentally determined from the CT reconstruction of the beam, while the true FWHM data are those required to produce the CT-reconstructed value for a given slit width.

The true FWHM value was back-calculated using an iterative procedure from the tomographically reconstructed (measured) FWHM of the beam, the slit width, and Equations 3–5. The error in the FWHM measurement represents the percentage that the CT reconstruction overestimates the true FWHM of the beam, as calculated from the difference between the true and measured FWHM values.

These results show the 0.1-mm-wide slit produces errors between 3.58 and 14.9%, while the double-wide slit produces significantly higher errors, between 18.0 and 102% in the FWHM of these different beams. It is clear the amount of error introduced into the FWHM measurement by the 0.2-mm-wide slit is excessive for small-diameter beams. Furthermore, the fact that not all the slits in the tungsten slit disk are the same size makes it difficult to properly compensate for the effect of slit width on the CT-reconstructed beam. Because of this potential error, we investigated a new method for orienting the beam using 17 small, uniform slit widths that would allow the amount of error in the CT reconstruction to be more accurately predicted.

Table 3 — Amount of Error in Measured FWHM Values of Sharp-Focused, 5-mA Beams as a Result of Different Slit Widths

EB Welding Machine	Voltage (kV)	Slit Width (mm)	Measured FWHM (mm)	True FWHM (mm)	R	Error (E_{FWHM}) (%)
No. 605	140	0.1	0.280	0.270	0.370	3.58
No. 175	60	0.1	0.260	0.250	0.400	4.12
No. 175	140	0.1	0.150	0.131	0.763	14.9
No. 605	140	0.2	0.280	0.237	0.843	18.0
No. 175	60	0.2	0.260	0.212	0.943	22.5
No. 175	140	0.2	0.150	0.074	2.70	102

Note: Results are from two different welding machine, and for different accelerating voltages.

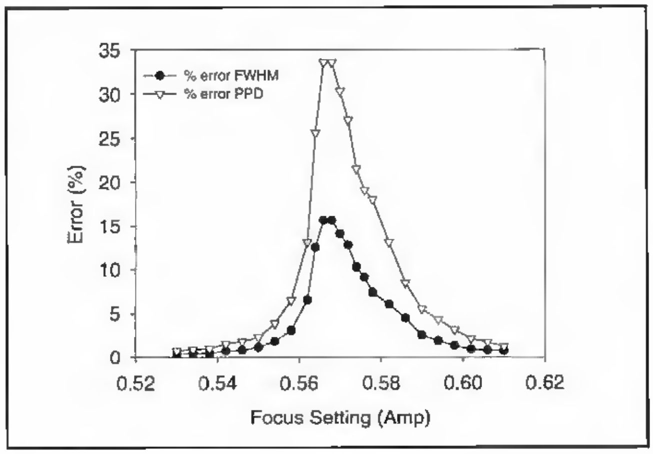

Fig. 9 — Percentage error in the FWHM and peak power density measurements caused by the 0.1-mm-wide slit as a function of focus setting for the 140-kV, 5-mA beam on HS welding machine No. 175.

Determining Beam Orientation Using Equal Width Slits

The original 17 slit tungsten disk design is illustrated in Fig. 7A. In this design, the slits are equally spaced at 21.18 deg, giving an equivalent spacing of 10.59 deg per beam profile in the reconstructed beam (Ref. 8). The beam orientation is determined using one wide slit (0.2 mm) (Ref. 8), which can produce a large error in the beam profile as discussed above.

The new tungsten slit design is illustrated in Fig. 7B. In this design, all of the slits are machined with the same width (0.1 mm) to reduce the amount of error introduced into the CT reconstruction, and the beam orientation is determined with one wide-spaced set of slits.

The spacing of the wide slit was chosen to be as small as possible to keep the overall spacing of the remaining slits as regular as possible. Here, we chose 24 deg for the wide-spaced slit, which produced enough of a temporal gap in the acquired data waveform for the sharp-focused and defocused beams investigated in this study to be characterized.

The remainder of the slits were equally spaced at 21 deg. This nonregular slit spacing required only minor changes to be made to the CT algorithm for reconstructing the beam. Since this disk also contained 17 slits, the CT reconstruction was performed with the same average angular resolution as that of the original slit disk design.

Using the new tungsten slit disk design, a 140-kV, 5-mA beam was investigated through a range of focus settings of ±0.040 A. This beam was shown to have a measured FWHM of 0.148 mm at sharp focus, which corresponds to a corrected true FWHM value of 0.128 mm. Waveform analysis of raw data was performed in preparation of tomographic reconstruction and showed the wide angle was able to be distinguished in the 17-slit waveform for both sharp-focused and defocused beams (±0.040 A). Thus the

Table 4 — Summary of Properties for a 140 kV, 5 mA Electron Beam on HS No. 175 Welding Machine as a Function of Defocus

Focus Setting (A)	Relative Focus (mA)	Measured FWHM (mm)	Measured FWe2 (mm)	Measured PPD (kW/mm²)	True FWHM (mm)	Corrected PPD (kW/mm²)
0.530	–38	1.009	1.238	1.01	1.005	1.02
0.534	–34	0.895	1.130	1.27	0.891	1.28
0.538	–30	0.814	1.006	1.54	0.810	1.55
0.542	–26	0.649	0.853	2.19	0.644	2.23
0.546	–22	0.586	0.757	2.75	0.581	2.80
0.550	–18	0.509	0.652	3.63	0.503	3.72
0.554	–14	0.384	0.514	5.79	0.377	6.01
0.558	–10	0.297	0.415	9.16	0.288	9.75
0.562	–6	0.212	0.327	13.72	0.199	15.52
0.564	–4	0.162	0.267	23.74	0.144	29.81
0.566	–2	0.148	0.258	26.68	0.128	35.63
0.568	0	0.148	0.253	26.09	0.128	34.84
0.570	2	0.154	0.262	24.28	0.135	31.63
0.572	4	0.159	0.281	21.06	0.141	26.75
0.574	6	0.172	0.296	18.56	0.156	22.55
0.576	8	0.180	0.320	15.98	0.165	19.03
0.578	10	0.180	0.331	15.05	0.165	17.81
0.582	14	0.212	0.400	10.43	0.199	11.79
0.586	18	0.257	0.499	7.01	0.246	7.60
0.590	22	0.322	0.644	4.42	0.314	4.66
0.594	26	0.372	0.738	3.39	0.365	3.54
0.598	30	0.444	0.891	2.42	0.438	2.50
0.602	34	0.539	1.043	2.11	0.534	2.16
0.606	38	0.607	1.149	1.48	0.602	1.50
0.610	42	0.681	1.273	1.21	0.676	1.23

Note: The true FWHM and corrected peak power density (PPD) for each condition are derived from the measured values and slit width of 0.1 mm.

wide angle was capable of being identified and the data was capable of being tomographically reconstructed, while at the same time retaining the orientation of the beam.

The results of the defocus study are summarized in Table 4 for the 25 different focus settings. In this table, the measured FWHM, measured FWe2, and measured PPD data refer to the data as tomographically reconstructed prior to correction of the finite width of the slit.

The results of the defocus study are plotted in Fig. 8A (FWHM) and 8B (peak power density). Two sets of data are presented in each figure. The solid circles represent tomographically reconstructed beam parameters, while the open circles represent these same data after correction of errors introduced by the finite width of the slit.

Looking first at the uncorrected FWHM data in Fig. 8A (solid circles), the FWHM values reach a minimum value of 0.148 mm at the 0.568-A setting, where the highest peak power density is achieved. As the beam is defocused, the FWHM increases to values as high as 1.0 mm at the 0.530-A focus setting (–0.038-A defocus).

There is clearly an asymmetry in the overall defocus curve, whereby the beam defocuses to wider FWHM values (and correspondingly lower peak power densities) more rapidly as the beam is defocused above the tungsten slit (focus settings less than 0.568) than below. The peak power density measurements shown in Fig. 8B indicate this beam has a peak of 26 kW/mm² for the sharpest focused beam (focus setting 0.568 A), but drops off to values near 1 kW/mm² for the defocused beams.

Error Corrections for 0.1-mm-Wide Slits

The tomographically reconstructed (measured) data shown by the solid circles in Fig. 8 represents an overestimate of the beam dimensions due to the finite width of the slit. It is possible to account for this error by back-calculating the true FWHM from the reconstructed (measured) FWHM values as described in the previous section. These calculations were performed on each data point and are summarized in Table 4.

The true FWHM data are plotted as a function of defocus setting as the open circles in Fig. 8A. The major differences between the corrected and uncorrected FWHM values occur for the sharpest focused beams, in a 0.020-A range of defocus settings from 0.560 to 0.580 A. For data outside this range, the two curves nearly merge together, indicating the measured and true FWHM data are nearly the same.

To provide a clearer picture of the difference between the corrected and uncorrected FWHM values, Fig. 9 plots the amount of error in the FWHM value as a function of defocus setting (solid circles). These data indicate the error in FWHM caused by 0.1-mm-wide slits increases from less than 1% for the most defocused beams to about 15% for the sharpest focused beam.

The error in the FWHM measurement introduced by the finite width of the slit corresponds to an even larger error in the peak power density. This error can be calculated using Equation 1, which shows the peak power density is inversely proportional to the square of the standard deviation of the beam, and thus is inversely proportional to the square of FWHM. Using this relationship, the peak power density measurements were corrected for adjustment with the true FWHM dimension of the beams. These data are plotted as open circles in Fig. 8B and indicate the corrected peak power densities are significantly higher than the uncorrected values in the sharp-focus region of the beam (0.560 to 0.580 A). Figure 9 further plots the amount of error in the peak power density measurements (open circles) as a function of defocus setting, indicating the error increases from values around 1% for the most defocused beams to 33% for the sharpest focused beam.

In summary, errors in the measured FWHM values introduced by the finite width of the slit are most severe for small-diameter beams, and these errors in FWHM result in even larger errors in the reconstructed power density distribution of the beam. These known errors for Gaussian-distributed beams are on the order of 5% in FWHM and 10% in the peak power density for beams with R values of 0.4, and increase rapidly as R increases. Mathematical corrections can be made to adjust for the error in the tomographically measured beam parameters knowing the width of the slits. These corrections are particularly important when transferring parameters between machines, studying beam/material interactions, and comparing beam-profiling results when different MFC devices have been used.

Conclusions

1) An enhanced MFC was designed and used to measure total beam current and power density distribution for high-power electron beams used in welding.

2) The enhanced MFC demonstrated improved electron capture over the original MFC and resulted in capturing, on average, 99% of the electron beam.

3) A new method for orienting the electron beam was developed using one set of wide-spaced slits rather than the

one wide slit used in the past. This new method for beam orientation allowed all the slits to be machined with the same (small) slit width of 0.1 mm, which eliminated the large error caused by the double-wide slit used in the past.

4) Calculations were performed to simulate beam profiles as measured by slits of various widths. Results showed slit widths of 0.1 mm overestimate the measured FWHM values by amounts up to 15% for small-diameter, sharp-focused beams. This FWHM error corresponds to an underestimation of the peak power density by 33% for these same beams. The errors drop off quickly for larger-diameter beams.

5) A method was developed to compensate for beam size error introduced by the finite width of the slits. This method assumes the beam has a Gaussian distribution, which is a reasonable assumption for sharp-focused beams. Corrections were made to the CT reconstructions of a 140-kV, 5-mA beam through a wide range of defocus settings. These corrections are particularly important when the ratio of the slit width to the true FWHM value of the beam, R, is larger than 0.4, where the error in FWHM is greater than 5% and the error in the peak power density is greater than 10% of its true value before performing the correction.

Acknowledgments

The authors acknowledge and appreciate the assistance of Mark Gauthier for performing the electron beam welding. The authors would also like to acknowledge T. Mustaleski of the BWXT Y-12 plant, and J. Dereskiewicz of the Honeywell Kansas City plant for many helpful discussions about introducing electron beam profiling into production settings. This work was performed under the auspices of the U.S. Department of Energy by the University of California, Lawrence Livermore National Laboratory under Contract No. W-7405-Eng-48.

References

1. *Recommended Practices for Electron Beam Welding*. 1992. ANSI/AWS C7.1-92. Miami, Fla.: American Welding Society.

2. Tallerico, L. N., and Giedt, W. H. 1988. *Welding Journal* 67(12): 299-s to 305-s.

3. Hicken, G. K., Giedt, W. H., and Bentley, A. E. 1991. *Welding Journal* 70(3):69-s to 75-s.

4. Arata, Y. 1986. *Plasma, Electron and Laser Beam Technology*. Materials Park, Ohio: ASM International, pp. 3–27.

5. Dilthey, U., and Weiser, J. 1995. *Schw. und Schn.* 47(7): 558–564.

6. *Ibid*. pp. 339–345.

7. LaFlamme, G. R., and Powers, D. E. 1991. *Welding Journal* 70(10): 33–40.

8. Elmer, J. W., and Teruya, A. T. 1998. Fast method for measuring power-density distribution of non-circular and irregular electron beams. *Science and Technology of Welding and Joining* 3(2): 51.

9. Elmer, J. W, Teruya, A. T., and O'Brien, D. W. 1993. *Welding Journal* 72(11): 493-s to 505-s.

10. Teruya, A. T., Elmer, J. W., and O'Brien, D. W. 1991. *The Laser and Electron Beam in Welding, Cutting, and Surface Treatment — State-of-the-Art 1991*. Bakish Materials Corp., pp. 125–140.

11. National Instruments Corp., *LabView* version 6.0 for Windows™, 2000 edition.

12. MathSoft Engineering & Education, Inc. *Mathcad* 2000, Professional edition.

Preparation of Manuscripts for Submission to the *Welding Journal* Research Supplement

All authors should address themselves to the following questions when writing papers for submission to the Welding Research Supplement:

- ◆ Why was the work done?
- ◆ What was done?
- ◆ What was found?
- ◆ What is the significance of your results?
- ◆ What are your most important conclusions?

With those questions in mind, most authors can logically organize their material along the following lines, using suitable headings and subheadings to divide the paper.

1) **Abstract.** A concise summary of the major elements of the presentation, not exceeding 200 words, to help the reader decide if the information is for him or her.

2) **Introduction.** A short statement giving relevant background, purpose and scope to help orient the reader. Do not duplicate the abstract.

3) **Experimental Procedure, Materials, Equipment.**

4) **Results, Discussion.** The facts or data obtained and their evaluation.

5) **Conclusion.** An evaluation and interpretation of your results. Most often, this is what the readers remember.

6) **Acknowledgment, References, and Appendix.**

Keep in mind that proper use of terms, abbreviations, and symbols are important considerations in processing a manuscript for publication. For welding terminology, the *Welding Journal* adheres to ANSI/AWS A3.0-94, *Standard Welding Terms and Definitions.*

Papers submitted for consideration in the Welding Research Supplement are required to undergo Peer Review before acceptance for publication. Submit an original and one copy (double-spaced with 1-in. margins on 8 ½ x 11-in. or A4 paper) of the manuscript. Submit the abstract only on a computer disk. The preferred format is from any Macintosh® word processor on a 3.5-in. double- or high-density disk. Other acceptable formats include ASCII text, Windows™, or DOS. A manuscript submission form should accompany the manuscript.

Tables and figures should be separate from the manuscript copy and only high-quality figures will be published. Figures should be original line art or glossy photos. Special instructions are required if figures are submitted by electronic means. To receive complete instructions and the manuscript submission form, please contact the Peer Review Coordinator, Doreen Kubish, at (305) 443-9353, ext. 275; FAX 305-443-7404; or write to the American Welding Society, 550 NW LeJeune Rd., Miami, FL 33126.